

Title: Dynamic Kernel Evolution in the Entropy-Decay Curvature Framework and Its Manifestation in Graphene Transport

Author: Louis Hin Lok Tsang
Affiliation: Independent Researcher, Birmingham, UK
Email: louis_hlt@tsangentropydecay.org.uk
Revision: 1.0
Publish date: 13/05/2026

Abstract:

The entropy-decay curvature framework was originally developed from the Tsang equation, in which entropy progression is governed through curvature in decay evolution across structural, wave-like, and stochastic propagation channels. Subsequent work extended the framework through a memory-embedded formulation, where historical system behaviour contributes through stationary interaction kernels defined relative to the onset of irreversible subsystem exchange. This stationary-kernel approximation was sufficient for describing stable regimes in which observable material behaviour remains approximately linear and dynamically consistent over time.

In the present work, the framework is further extended by promoting the stationary memory kernel into a dynamically evolving non-stationary effective kernel emerging from subsystem interaction between material, environmental, and external drive components. The extension is motivated by the observation that stationary formulations become insufficient near localized transition regimes, where the interaction structure itself evolves and the effective kernel can no longer be treated as constant. In this interpretation, relaxation, threshold behaviour, and transition anomalies are treated as emergent consequences of kernel evolution rather than as independent dissipative corrections external to the entropy-decay curvature dynamics.

The formalism is applied to graphene transport near the Dirac point using previously reported experimental datasets. Multiple observables, including minimum conductivity behaviour, Lorenz ratio variation, viscosity-to-entropy scaling, and thermal smearing proxies, exhibit synchronized anomalies within a localized transition window between 60 K and 110 K. These features are interpreted as signatures of non-stationary effective kernel evolution associated with threshold-driven regime change rather than conventional equilibrium phase transition alone. The effective kernel memory scale, extracted from minimum conductivity as the dimensionless ratio τ_m/τ_p , decreases monotonically from 0.901 at 90 K to 0.440 at 249 K following a power-law dependence $T^{-0.72}$, remaining sub-Planckian across the full measured range.

The present framework remains phenomenological in several respects and does not yet provide a first-principles derivation for the explicit evolution function governing the effective kernel. Nevertheless, it establishes a unified structure connecting entropy-decay curvature dynamics, subsystem interaction, memory effects, and transition behaviour within a single evolving-kernel formalism. The framework further suggests experimentally testable distinctions between stable and transition regimes through the behaviour of kernel variation with respect to decay progression and interaction structure.

Keywords:

Entropy-decay dynamics; Non-stationary memory kernels; Graphene transport; Quantum critical behaviour; Subsystem interaction formalism; Transition regime evolution;

1. Foundations of the Entropy-Decay Curvature Framework

Recent experimental investigations of strongly interacting transport systems, particularly in ultraclean

graphene and related low-dimensional materials, have revealed transport behaviour that deviates systematically from simple stationary scattering descriptions. Observed phenomena including hydrodynamic electron flow [6,13], synchronized transport anomalies, non-monotonic conductivity evolution, violation of conventional Wiedemann–Franz scaling [5,7], and localized crossover behaviour suggest that transport response in such systems depends not only on instantaneous subsystem conditions, but also on accumulated interaction history and evolving propagation structure. Recent numerical modelling by Patel et al. of two-dimensional metals with spatially disordered interactions has found that Planckian-scale transport scattering rates may emerge from an extended gapless phase rather than from a conventional quantum critical point, with the scattering rate remaining independent of coupling strength across the strange-metal regime [4]. While that work proceeds from a specific microscopic spin-fermion model rather than from experimental measurement, its findings are broadly consistent with the interpretation that accumulated interaction history and evolving subsystem coupling structures contribute to transport behaviour in strongly interacting systems. These considerations motivate the development of phenomenological frameworks capable of describing transport evolution beyond purely local or stationary approximations.

Within the present entropy-decay curvature framework [1,2], the fundamental state quantity is represented by $S(\tau, \Psi)$, describing the entropy state of a subsystem as a function of decay progression τ and interaction structure Ψ . Unlike conventional thermodynamic entropy defined primarily through equilibrium statistical interpretation, $S(\tau, \Psi)$ is treated here as a dynamical state function capable of evolving across structural, propagative, and stochastic transport regimes. In this interpretation, entropy is not treated solely as equilibrium disorder, but as an evolving interaction state associated with irreversible subsystem exchange and propagation behaviour.

The foundational relation of the framework is the Tsang equation:

$$\frac{\partial^2 S}{\partial \tau^2} = \alpha \nabla_{\Psi}^2 S + \beta \frac{\partial^2}{\partial \tau^2} (\nabla_{\Psi}^2 S) + \gamma \sum_n \xi_n \Lambda_n(\tau)$$

In this formulation, S represents the entropy state of the subsystem, while τ denotes decay progression rather than conventional external clock time. The coordinate Ψ represents the interaction structure associated with subsystem configuration and propagation environment. The left-hand side describes curvature in entropy-decay progression, while the right-hand side contains three coupled propagation contributions governing structural, scattering-mediated, and stochastic subsystem behaviour.

The coefficient α represents structural or material-response behaviour associated with interaction structure curvature and spatial propagation. The β contribution describes scattering-mediated and wave-like propagation behaviour in which entropy-decay progression and interaction-structure evolution occur simultaneously. The stochastic contribution represented through $\gamma \sum_n \xi_n \Lambda_n(\tau)$ incorporates fluctuating, radiative, or probabilistic propagation channels associated with unresolved subsystem exchange. These contributions are not interpreted as fundamentally separate physical substances, but as coupled observable manifestations of the same underlying entropy-decay propagation dynamics.

Within the present framework, observable transport behaviour may emerge through effective channels including thermal transport, electrical conduction, scattering response, radiative exchange, collective flow behaviour, and mechanical propagation. The total observable entropy state may therefore be represented schematically as:

$$S(\tau, \Psi) = \sum_i S_i(\tau, \Psi)$$

where the individual components correspond to effective observable representations of subsystem response under specific interaction-structure conditions. These channels are not interpreted as independent entropy substances, but as observational decompositions of a unified entropy-decay propagation process.

An important consequence of the framework is that stable observable physics emerges primarily through approximately stationary entropy-decay transport regimes. When the governing interaction structure evolves negligibly over the observational interval, subsystem behaviour exhibits smooth and often approximately linear observable response. Many conventional equilibrium and near-equilibrium transport descriptions therefore remain effective approximations within stable regimes. The underlying subsystem interaction history nevertheless remains present implicitly, and its influence becomes experimentally accessible when the stationary approximation breaks down near localized transition conditions.

Experimental transport anomalies observed in strongly interacting systems suggest that this stationary approximation may become insufficient near such localized transition regimes. In particular, synchronized deviations across multiple transport observables near graphene charge-neutrality conditions, combined with the emergence of Planckian-scale transport timescales [8] in systems with disordered interactions, motivate the possibility that the interaction structure governing subsystem propagation may itself evolve during transport progression. The present work therefore extends the original entropy-decay curvature framework through a memory-embedded and dynamically evolving interaction-kernel formalism capable of describing non-stationary subsystem interaction behaviour near localized transition conditions, and applies it to previously reported transport measurements in ultraclean graphene to identify signatures of this evolution across four independent transport observables.

2. Memory-Embedded Formalism

While the original Tsang equation describes local entropy-decay curvature dynamics, it does not explicitly incorporate historical subsystem interaction or delayed propagation effects accumulated during irreversible exchange. Many experimentally accessible transport systems exhibit behaviour suggesting that subsystem response depends not solely on instantaneous state conditions, but also on accumulated interaction history. Structural relaxation, transport hysteresis, thermal retention, delayed scattering response, and collective propagation behaviour all indicate that prior subsystem exchange may continue influencing subsequent transport evolution over finite decay intervals. These observations motivate an extension of the entropy-decay curvature framework through a memory-embedded formalism [10,11,12] in which prior subsystem states contribute to present behaviour through an interaction-weighting kernel acting across the history of subsystem exchange.

2.1 Stationary Memory-Embedded Formalism

Under the stationary approximation, the memory-embedded entropy-decay equation may be expressed as:

$$\begin{aligned} \int_{\tau_{\text{exchange}}}^{\tau} K(\tau - \tau') \frac{\partial^2 S(\tau', \Psi)}{\partial \tau^2} d\tau' &= \alpha \int_{\tau_{\text{exchange}}}^{\tau} K(\tau - \tau') \frac{\partial^2 S(\tau', \Psi)}{\partial \Psi^2} d\tau' \\ &+ \beta \int_{\tau_{\text{exchange}}}^{\tau} K(\tau - \tau') \frac{\partial^4 S(\tau', \Psi)}{\partial \Psi^2 \partial \tau^2} d\tau' + \gamma \int_{\tau_{\text{exchange}}}^{\tau} K(\tau - \tau') \sum_n \xi_n \Lambda_n(\tau') d\tau' \end{aligned}$$

In this formulation, $K(\tau - \tau')$ represents a stationary interaction-weighting kernel governing the relative contribution of prior subsystem states to present entropy-decay evolution. The lower integration boundary τ_{exchange} denotes the onset of irreversible subsystem exchange rather than an absolute universal origin. The formalism is therefore subsystem-relative and depends on the initiation of relevant interaction history between coupled structures or environments.

Under the stationary approximation, the kernel depends only on the relative separation $(\tau - \tau')$ between past and present decay progression, and not on the evolving state of the subsystem itself. This corresponds physically to regimes in which the interaction structure governing entropy propagation remains approximately stable over the observational interval, so that observable behaviour evolves smoothly and

often exhibits approximately linear or weakly nonlinear response characteristics. Within such stable regimes, the stationary memory-kernel approximation remains sufficient to describe delayed subsystem response, and many conventional near-equilibrium transport descriptions may be interpreted phenomenologically as limiting cases of this stationary formalism [12].

2.2 Kernel Variation and Transition Regimes

To characterise the boundary between stable and transition-sensitive transport behaviour, the framework introduces kernel variation with respect to both decay progression and interaction structure:

$$\frac{dK}{d\tau} \text{ and } \frac{dK}{d\Psi}$$

These quantities are not interpreted as conventional thermodynamic derivatives, but as phenomenological indicators describing how the effective subsystem interaction weighting evolves as the system progresses through changing decay conditions and interaction-structure configurations.

Within stable transport regimes, both quantities remain negligible:

$$\frac{dK}{d\tau} \approx 0, \text{ and } \frac{dK}{d\Psi} \approx 0$$

Under these conditions, the interaction-weighting structure remains approximately stationary, observable transport coefficients evolve smoothly, and conventional transport approximations remain effective over finite observational intervals. Stability here does not imply thermodynamic equilibrium, but rather the relative constancy of the governing interaction-weighting structure over the relevant observational interval.

Near localized transition regimes, however, kernel variation may become non-negligible. A non-zero value of $dK/d\tau$ indicates that subsystem interaction weighting evolves as the system progresses through entropy-decay evolution, physically corresponding to situations in which subsystem memory and propagation response are no longer temporally stable. A non-zero value of $dK/d\Psi$ indicates that the interaction structure itself evolves across the subsystem configuration landscape, so that entropy propagation no longer occurs through a fixed interaction geometry but through a dynamically shifting propagation structure.

This distinction carries a physically important consequence. Observable transport suppression may arise in two fundamentally different ways: either because the subsystem has not accumulated sufficient interaction history to destabilise the existing transport regime, or because incoming propagation channels fail to couple efficiently with the subsystem's internal decay progression despite sufficient external drive magnitude. Although these situations may produce superficially similar observable behaviour, the underlying interaction structures governing subsystem propagation differ fundamentally and may require different external interventions to alter the transport response. The experimental signatures distinguishing these two mechanisms are examined in Section 6 in the context of the graphene transport analysis.

The introduction of $dK/d\tau$ and $dK/d\Psi$ therefore extends the stationary memory formalism into a transition-sensitive entropy-decay framework. The stationary kernel equation remains valid as the limiting case in which kernel variation is negligible. Non-stationary kernel evolution emerges only under restricted transition-sensitive conditions, rather than as unrestricted fluctuation across all transport regimes, and it is precisely this localised character that makes the resulting transport anomalies experimentally identifiable as distinct from ordinary smooth evolution.

3. Subsystem Interaction and Effective Kernel Emergence

The stationary memory-embedded formalism developed in Section 2 treats the subsystem as evolving under a fixed historical weighting structure. This approximation captures delayed propagation effects within stable

transport regimes but does not account for the possibility that the interaction structure itself may evolve during subsystem exchange. To address this, the present section introduces explicit subsystem decomposition, derives the effective interaction kernel from first principles within the entropy-decay curvature framework, and establishes the conditions under which that kernel transitions from stationary to non-stationary behaviour.

3.1 Subsystem Decomposition

Rather than treating the observed system as evolving in isolation, the framework considers entropy propagation as arising through coupled interaction between multiple subsystem environments contributing simultaneously to the observed transport behaviour. For the graphene transport system considered in the present work, three dominant subsystem contributions are identified: the graphene subsystem G , the environmental background subsystem E representing slowly varying thermal and laboratory conditions, and the external drive subsystem D associated with the applied current source.

The governing entropy-decay curvature relation for the graphene subsystem under coupled interaction may be written as:

$$\frac{\partial^2 S_G}{\partial \tau_G^2} = \int K_{GE}(\tau_G - \tau')[S_E - S_G(\tau')]d\tau' + \int K_{GD}(\tau_G - \tau')[S_D(\tau') - S_G(\tau')]d\tau' + \gamma_G \sum_n \xi_n \Lambda_n(\tau')$$

Here S_G represents the entropy state of the graphene subsystem, S_E the environmental background contribution, and S_D the externally driven transport contribution. The coupling kernels K_{GE} and K_{GD} weight the historical interaction contributions between graphene and each respective subsystem over decay progression. The stochastic term retains its role as an active propagation channel whose relative significance varies across transport regimes, rather than acting as a residual correction external to the primary dynamics.

This formulation is not introduced as a microscopic derivation of material structure. Rather, it represents a phenomenological decomposition of experimentally observable transport contributions into coupled interaction channels. The kernels K_{GE} and K_{GD} therefore encode effective interaction weighting histories associated with environmental and driven transport coupling, and their introduction is justified by the observable fact that graphene transport measurements are performed under simultaneously active environmental and drive conditions that cannot be treated as decoupled from the subsystem response.

3.2 Reduction to the Effective Interaction Kernel

Over the observational interval of the transport measurements, both the environmental background subsystem and the externally driven current subsystem remain approximately stable relative to the evolving graphene response. The environmental subsystem varies slowly and may be approximated as a quasi-stationary background contribution C_E . The drive subsystem is experimentally controlled over finite intervals. Under these conditions, the dominant observable evolution emerges through the graphene subsystem response under coupled interaction weighting.

Collecting all graphene-dependent weighting contributions together from the subsystem equation:

$$\frac{\partial^2 S_G}{\partial \tau_G^2} = - \int (K_{GE} + K_{GD})(\tau_G - \tau')S_G(\tau')d\tau' + \int K_{GD}(\tau_G - \tau')S_D(\tau')d\tau' + C_E + \gamma_G \sum_n \xi_n \Lambda_n(\tau')$$

This regrouping naturally motivates the definition of an effective interaction kernel:

$$K_{eff} = K_{GE} + K_{GD}$$

The effective interaction kernel therefore emerges directly from subsystem decomposition under experimentally constrained conditions. It is not introduced as an arbitrary fitting parameter. Rather, K_{eff} represents the consolidated interaction weighting structure governing the observable graphene transport

response under simultaneous environmental and driven subsystem coupling. Within stable transport regimes where both K_{GE} and K_{GD} evolve negligibly over the observational interval, K_{eff} reduces to a stationary kernel $K_{eff}(\tau - \tau')$ and the earlier memory-embedded formalism of Section 2 is recovered naturally as a limiting case.

3.3 Promotion to a Non-Stationary Kernel

Near localized transition conditions, the effective interaction kernel can no longer be treated as stationary. The kernel is promoted from dependence solely on historical separation to explicit dependence on both historical separation and present decay progression:

$$K_{eff}(\tau - \tau') \rightarrow K_{eff}(\tau - \tau', \tau)$$

This promotion does not imply unrestricted or arbitrary kernel fluctuation. Within the present interpretation, kernel evolution remains localized and limited to specific threshold or resonance regimes. For the majority of experimentally accessible intervals, the interaction kernel remains approximately stationary and the stable-regime approximation continues to hold. Observable non-stationary behaviour therefore emerges primarily near localized transition regions where subsystem interaction weighting becomes sensitive to accumulated environmental coupling or propagation mismatch.

The full non-stationary memory-embedded entropy-decay equation may now be written as:

$$\begin{aligned} \int K_{eff}(\tau - \tau', \tau) \frac{\partial^2 S(\tau', \Psi)}{\partial \tau'^2} d\tau' &= \alpha(K) \int K_{eff}(\tau - \tau', \tau) \frac{\partial^2 S(\tau', \Psi)}{\partial \Psi^2} d\tau' \\ &+ \beta(K) \int K_{eff}(\tau - \tau', \tau) \frac{\partial^4 S(\tau', \Psi)}{\partial \Psi^2 \partial \tau'^2} d\tau' + \gamma(K) \int K_{eff}(\tau - \tau', \tau) \sum \xi_n \Lambda_n(\tau') d\tau' \end{aligned}$$

The notation $\alpha(K)$, $\beta(K)$, $\gamma(K)$ indicates that the relative weighting of structural, scattering-mediated, and stochastic propagation contributions depends on the state of the effective kernel. This is not a claim that these coefficients are arbitrary functions of K , but rather that their effective values within a given transport regime are set by the stability and character of the governing interaction weighting structure, as developed in Section 4.

The kernel variation indicators introduced in Section 2.2 now acquire precise operational meaning within this equation. When $dK/d\tau \approx 0$ and $dK/d\Psi \approx 0$ the kernel is effectively stationary, the above equation reduces to the stationary formalism, and conventional transport descriptions emerge as limiting approximations. When either quantity becomes non-negligible, the weighting of the three propagation channels shifts, and observable transport anomalies emerge as consequences of that shift rather than as independent dissipative corrections.

3.4 Two Transition Mechanisms

Within this framework, two physically distinct mechanisms can initiate non-stationary kernel evolution, and distinguishing between them has direct experimental consequences examined in Section 6.

The first is threshold-induced kernel evolution. Here, accumulated subsystem interaction progressively destabilises the existing interaction weighting structure. The effective kernel evolves because the history of environmental and drive coupling has accumulated sufficiently to shift the balance between K_{GE} and K_{GD} beyond what the stationary approximation can sustain. Observable transport anomalies emerge gradually as the subsystem approaches the transition-sensitive interval, and recovery following the transition is similarly gradual.

The second is resonant kernel coupling. Here, the incoming propagation structure becomes compatible with the internal decay progression governing subsystem response, producing enhanced kernel evolution even under comparatively limited accumulated interaction history. Observable anomalies emerge more abruptly

and within narrower sensitivity windows. Recovery is sharper because the mechanism depends on propagation compatibility rather than progressive environmental accumulation.

Both mechanisms produce externally similar transport suppression, but their dependence on interaction history and propagation structure differs fundamentally. The framework therefore predicts that systematic variation of external drive frequency, loading rate, and subsystem geometry should allow experimental separation of the two contributions, proposing a prediction developed quantitatively in Section 6.

4. Emergent Response Quantities, the Effective Timescale, and Stable Regime Formation

The preceding section established the non-stationary effective kernel as the governing structure of the entropy-decay curvature framework near transition-sensitive transport conditions. The present section addresses three questions that must be answered before the framework can make contact with experimental data.

1. How do observable transport quantities such as conductivity, Lorenz ratio, viscosity, thermal smearing emerge as response descriptors within this formalism?
2. How is the effective memory timescale τ_m extracted quantitatively from minimum conductivity, and how does it relate to the Planckian thermal timescale $\tau_p = \hbar/k_{BT}$?
3. What conditions define a stable transport regime and how does the framework account for the smooth behaviour observed outside the transition window?

4.1 Emergent Response Descriptors

Within the entropy-decay curvature framework, observable transport quantities do not exist independently of the interaction-weighting regime that produces them. They are not inputs to the framework but outputs of it, emergent descriptors that take well-defined effective values only when the governing kernel structure is sufficiently stable over the observational interval.

This emergence follows directly from the structure of the non-stationary memory-embedded equation developed in Section 3. When K_{eff} evolves negligibly over the observational interval, the three propagation contributions on the right-hand side of the Tsang equation stabilise into approximately constant effective channels. The structural propagation contribution governed by $\alpha(K)$ produces observable behaviour associated with lattice-mediated and spatially distributed transport response. The scattering-mediated contribution governed by $\beta(K)$ produces observable behaviour associated with collective propagation, non-local interaction, and scattering persistence. The stochastic contribution governed by $\gamma(K)$ produces observable behaviour associated with fluctuating, radiative, or unresolved propagation channels. These three channels are not independent physical substances. They are observational facets of the same underlying entropy-decay propagation process, whose relative visibility depends entirely on the stability and character of the governing kernel.

The regime-dependence of this emergence has a direct physical consequence for graphene near the Dirac point. The structural contribution $\alpha(K)$ is comparatively suppressed by the two-dimensional planar geometry and high structural order of ultraclean devices. The stochastic contribution $\gamma(K)$ is suppressed by the absence of disorder-mediated scattering, confirmed experimentally by the absence of the D Raman peak and suppressed charge inhomogeneity in the Majumdar devices. Under these conditions, the scattering-mediated contribution $\beta(K)$ becomes the dominant observable propagation channel near charge neutrality. This suppression of competing channels is precisely what makes graphene near the Dirac point an unusually sensitive experimental environment: localized evolution of K_{eff} produces observable transport anomalies that would be masked by structural or stochastic contributions in conventional metallic systems. The four observables examined in Section 5: minimum conductivity, Lorenz ratio, viscosity-to-entropy ratio, and thermal smearing width, are each sensitive to different projections of $\beta(K)$ -dominated propagation

behaviour, which is why their synchronized anomalous behaviour within the 60–110 K window constitutes convergent evidence of kernel evolution rather than coincidental scatter.

4.2 The Kernel Memory Scale and Its Observational Correspondence

Within the entropy-decay curvature framework, the effective kernel K_{eff} carries an internal characteristic scale governing how rapidly the historical weighting of prior subsystem states attenuates with increasing separation from the present decay progression. This scale is not a clock time. It is a property of the kernel itself, a measure of how far back along the decay progression axis prior states continue to exert significant influence on present entropy propagation behaviour.

To make this internal scale tractable within the entropy-decay coordinate system, the simplest physically motivated kernel form is adopted:

$$K(\Delta\tau) = \left(\frac{1}{\tau_m}\right) \exp\left(\frac{-\Delta\tau}{\tau_m}\right)$$

where $\Delta\tau = \tau - \tau'$ is the separation between present and prior decay progression states, and τ_m is the characteristic decay scale of the kernel's memory. This exponential form is the simplest kernel consistent with two requirements: it assigns maximum weighting to the most recent prior states and attenuates monotonically with increasing historical separation. It makes no claim about the microscopic origin of the interaction weighting structure, and the extracted τ_m values should be understood as effective parameters characterising the dominant memory scale of the kernel rather than as uniquely determined microscopic quantities. Alternative kernel forms of oscillatory kernels with mild $dK/d\Psi$ modulation, would yield modified extraction procedures, and sensitivity to such alternatives represents an open direction for future refinement identified in Section 7.

The internal scale τ_m becomes observable only through its influence on measurable transport quantities. Within the framework, the minimum conductivity G_{min} at the charge neutrality point reflects the efficiency with which the effective interaction weighting structure transmits externally imposed entropy propagation through the graphene subsystem at suppressed carrier density. A larger τ_m corresponds to stronger and more persistent interaction memory, meaning prior subsystem states continue to contribute substantially to present propagation behaviour over longer decay intervals. This produces more efficient entropy propagation transmission and correspondingly higher minimum conductivity. A smaller τ_m corresponds to memory that is rapidly attenuated, meaning the kernel weighting collapses quickly toward instantaneous response, and entropy propagation efficiency at the charge neutrality point is reduced accordingly.

This relationship between kernel memory scale and propagation efficiency may be expressed within the framework as a proportionality between G_{min} and τ_m , mediated by the geometry of the experimental device channel and the quantum of conductance e^2/h which sets the natural scale for electrical entropy propagation in a two-dimensional system:

$$G_{\text{min}} \propto \frac{\tau_m \left(\frac{e^2}{h}\right) \left(\frac{W}{L}\right)}{\hbar}$$

where W/L is the aspect ratio of the device channel and \hbar is introduced purely as the dimensional bridge connecting the decay progression coordinate system to SI measurement units. This is the precise point at which the framework makes an observational correspondence between its internal coordinate τ and the external measurement system, and it is a correspondence, not a foundational identity. The factor \hbar does not mean that τ is clock time. It means that when an external observer measures conductance in SI units, the internal kernel scale τ_m is accessible through that measurement via the natural quantum of conductance. This correspondence is deliberate and limited: it connects one observable quantity to one internal framework parameter, leaving the broader question of how the full entropy-decay coordinate system maps onto conventional spacetime as an open problem explicitly identified in Section 7.2.

To express the extracted kernel scale in dimensionless form, and thereby make it comparable across different temperatures and device configurations, a reference scale is required. The natural external reference is the Planckian thermal scale:

$$\tau_p = \hbar/k_{BT}$$

This quantity is not part of the entropy-decay framework. It is an external observer's timescale, derived from the quantum of action and the available thermal energy, representing the minimum physically meaningful scattering interval in a quantum critical system as understood within conventional transport theory. It is introduced here solely as a measuring rod, a reference against which the internal kernel scale τ_m can be expressed as a dimensionless ratio: τ_m/τ_p .

This ratio is therefore an observational proxy. It answers the question: relative to the minimum quantum thermal scattering scale accessible to an external observer, how persistent is the effective interaction memory governing entropy propagation in the graphene subsystem? A ratio below unity indicates that kernel memory operates on a scale shorter than the Planckian thermal bound. A ratio approaching unity as temperature decreases indicates that kernel memory becomes increasingly comparable to the quantum thermal limit. A ratio that decreases with increasing temperature indicates that thermal fluctuations progressively overcome the interaction memory structure, weakening the kernel's historical weighting at higher temperatures.

The dimensionless ratio is extracted from measured minimum conductance as:

$$\frac{\tau_m}{\tau_p} = G_{min} \left(\frac{L}{W} \right) \frac{h}{4e^2}$$

The factor of four reflects the fourfold degeneracy of graphene's electronic structure arising from spin and valley degrees of freedom, which sets the proportionality between the measured conductance and the single-channel quantum of conductance within this system. This extraction yields a sequence of τ_m/τ_p values across the experimental temperature range that constitutes the primary quantitative test of the non-stationary kernel interpretation developed in Sections 3 and 4. The results of this extraction, and their interpretation within the framework, are presented in Section 5.4.

4.3 Stable Regime Formation

Observable material behaviour within the present framework emerges once the effective interaction weighting structure stabilises sufficiently that the three propagation contributions $\alpha(K)$, $\beta(K)$, $\gamma(K)$ remain approximately constant over the observational interval. Stable transport regimes are not perfectly static equilibrium states. They are comparatively persistent interaction-weighting configurations in which kernel evolution remains sufficiently limited that the emergent response descriptors of Section 4.1 retain approximately well-defined values over the relevant observational scale.

Small localized variations in K_{eff} may occur continuously within ordinary subsystem evolution without producing observable transport discontinuities. Stable regimes correspond to conditions in which such variations remain sufficiently constrained that the dominant propagation structure of the subsystem is effectively preserved. It is only when accumulated subsystem interaction or propagation mismatch becomes significant relative to the existing kernel stability that localized evolution becomes experimentally observable.

For the graphene transport system near the Dirac point, this threshold is crossed within the 60–110 K window identified in Section 5. Below approximately 60 K, the transport observables evolve smoothly and the stationary kernel approximation remains effective. Above approximately 110 K, the observables again evolve smoothly, consistent with the kernel having transitioned into a new approximately stationary regime at higher temperature. Within the window itself, the synchronized anomalous behaviour of four independent observables is interpreted as the experimental signature of the transition between these two stable regimes: a localized interval of non-stationary kernel evolution driven by the threshold; and resonant mechanisms

identified in Section 3.4, whose quantitative characterisation through the τ_m/τ_P proxy of Section 4.2 is the subject of Section 5.

5. Application to Graphene Transport Near the Dirac Point

The non-stationary effective kernel formalism developed in the preceding sections is applied here to previously reported experimental transport measurements in ultraclean graphene near the charge neutrality point. The dataset employed is that reported by Majumdar et al in the study of quantum critical flow of charge and heat in ultraclean graphene [3], including supplementary datasets as deposited with that publication.

5.1 Why Graphene Near the Dirac Point Provides a Sensitive Observable Environment

The suppression of competing propagation channels near graphene's charge neutrality point, and the consequent dominance of scattering-mediated $\beta(K)$ -governed transport behaviour, was established in Section 4.1 as the physical basis for treating ultraclean graphene as a sensitive experimental environment for observing non-stationary kernel evolution. That argument is not repeated here. The present section instead identifies the specific experimental configuration of the Majumdar dataset that makes this sensitivity accessible to quantitative analysis.

The experimental system consists of hexagonal boron nitride encapsulated monolayer graphene devices fabricated to ultraclean standards, with carrier mobilities reaching up to $650,000 \text{ cm}^2\text{V}^{-1}\text{s}^{-1}$ following low-temperature current annealing. Transport measurements span temperatures from approximately 19 K to 260 K across multiple device configurations of varying channel geometry and cleanliness. The absence of the D Raman peak and suppressed charge inhomogeneity n_{min} in the fabricated devices confirm the ultraclean conditions under which the stochastic $\gamma(K)$ propagation contribution remains comparatively suppressed, as required by the framework conditions established in Section 4.1.

Four transport observables are examined as independent proxy indicators of effective kernel evolution across this temperature range. Their physical interpretation within the entropy-decay curvature framework is developed in Section 5.2, and their synchronized anomalous behaviour within the 60–110 K transition window is presented in Section 5.3.

5.2 Observable Proxies for Effective Kernel Behaviour

Within the present framework, the effective interaction kernel K_{eff} is not directly observable as an isolated quantity. Its behaviour must be inferred indirectly through transport observables that reflect different aspects of the underlying interaction weighting structure. Four principal observable quantities extracted from the Majumdar dataset are examined as independent proxy indicators of effective kernel evolution across the experimental temperature range.

The minimum electrical conductivity at the charge neutrality point, G_{min} , reflects the efficiency of entropy propagation through graphene at suppressed carrier density. In the present framework, G_{min} is interpreted as a measure of how efficiently the effective interaction weighting structure transmits externally imposed entropy propagation through the graphene subsystem at the Dirac point.

The Lorenz ratio L/L_{WF} characterises the relative balance between thermal and electrical transport response. Significant deviation from the Wiedemann–Franz expectation [5,7] of unity indicates that thermal and electrical propagation channels are not governed by a common scattering structure, consistent with the presence of interaction-dominated transport behaviour extending beyond conventional diffusive scattering approximations.

The viscosity-to-entropy density ratio η/s , measured in units of the holographic bound $\hbar/4\pi k_B$ [9,16], reflects the effective resistance of the electron fluid to collective propagative reorganisation [14,15]. Within the

present framework, this quantity is interpreted as a measure of how strongly the effective interaction weighting structure resists entropy propagation redistribution under external drive.

The thermal smearing width n_0 normalised to temperature characterises how environmental background entropy propagation couples into the effective interaction structure of the graphene subsystem. Under stable kernel conditions in which environmental coupling scales linearly with temperature, the ratio n_0/T is expected to remain approximately constant across the experimental temperature range.

In stable kernel regimes, all four observables are expected to evolve smoothly and approximately consistently with conventional transport behaviour. Near localized transition regimes, synchronized deviation from smooth behaviour across multiple independent observables simultaneously would be phenomenologically compatible with non-stationary kernel evolution operating within the subsystem interaction structure.

5.3 Transport Behaviour and the Localized Transition Window

Examination of the four observable quantities across the experimental temperature range from 19 K to 260 K reveals behaviour consistent with stable kernel evolution across most of the accessible range, punctuated by a localized window of anomalous behaviour between approximately 60 K and 110 K in which all four observables deviate simultaneously from smooth monotonic evolution.

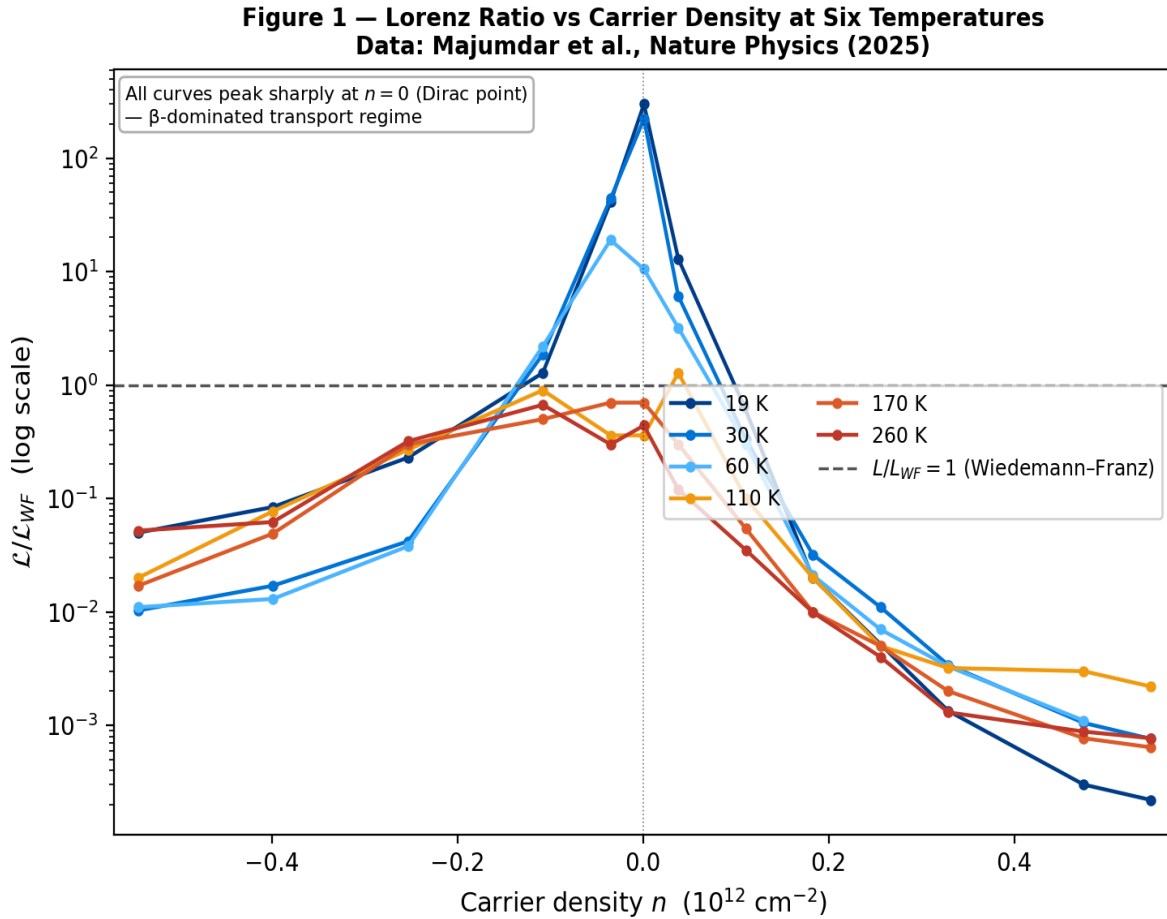


Figure 1: Lorenz Ratio versus carrier density at six temperatures.

Lorenz ratio behaviour: The Lorenz ratio at the charge neutrality point decreases from 300 at 19 K to 222 at 30 K, 19 at 60 K, and 1.28 at 110 K, before reaching 0.70 at 170 K and 0.44 at 260 K. As shown in Figure 1, all temperature curves peak sharply at the charge neutrality point $n = 0$, consistent with the β -dominated transport regime described in Section 5.1. The rate of decrease of the Lorenz ratio per Kelvin is not monotonic across the temperature range. The highest rate of decrease occurs between 30 K and 60 K at 0.082 per Kelvin, followed by a reduced rate of 0.054 per Kelvin between 60 K and 110 K, before declining

further to 0.010 per Kelvin between 110 K and 170 K and 0.005 per Kelvin between 170 K and 260 K. This non-monotonic rate behaviour, in which the rate of change is highest before the transition window rather than within or after it, is difficult to reconcile with simple monotonic diffusive scattering evolution alone. Panel A of Figure 2 presents the Lorenz ratio at the charge neutrality point across the full temperature range, with the 60–110 K transition window indicated.

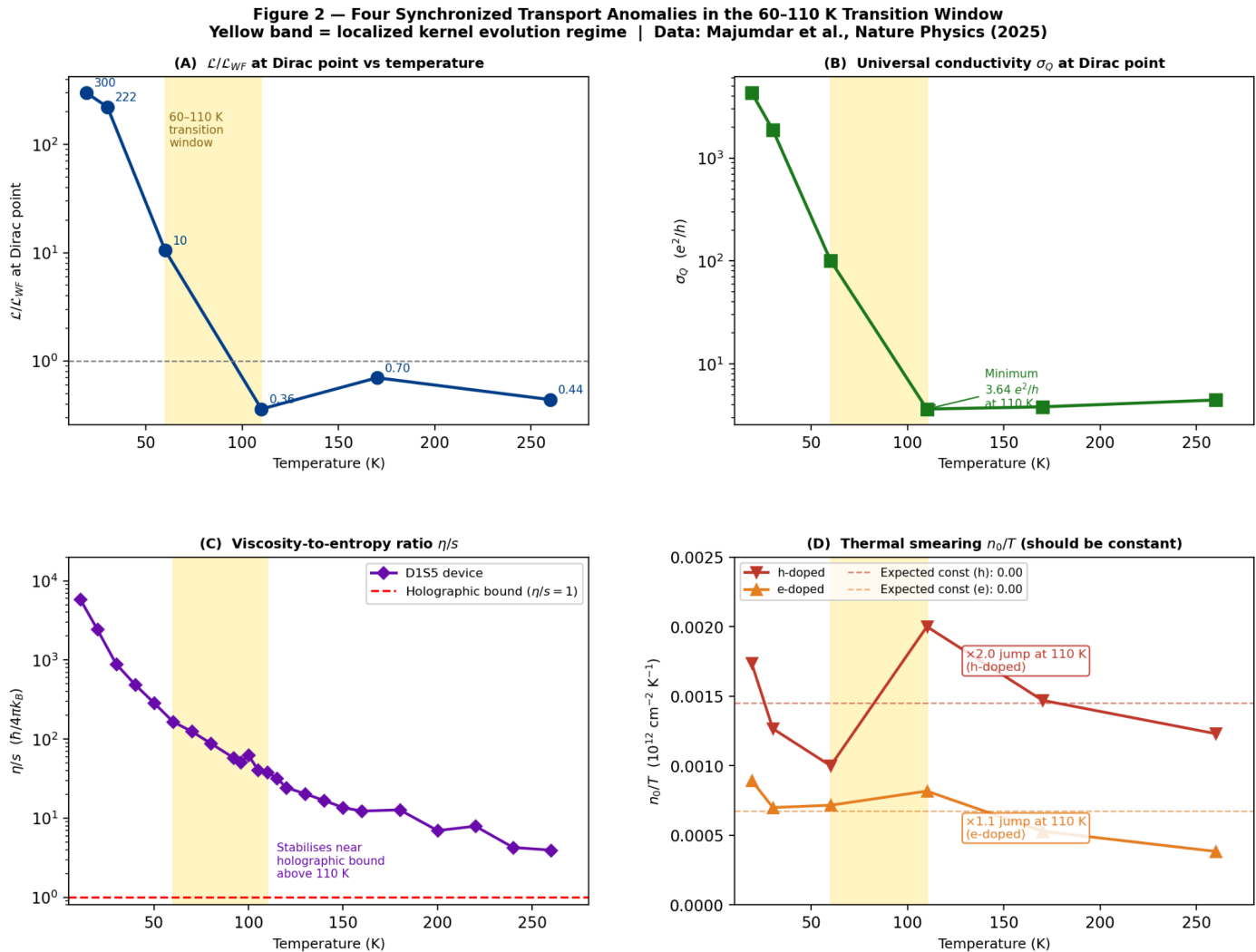


Figure 2: Four synchronized transport anomalies in the 60-110 K transition window.

Universal conductivity behaviour: The effective quantum conductivity σ_Q at the charge neutrality point, determined from combined electrical and thermal transport observables, decreases from 4309.5 e^2/h at 19 K through 1876.2 e^2/h at 30 K and 100.7 e^2/h at 60 K, reaching a minimum value of 3.64 e^2/h at 110 K before stabilising to 3.82 e^2/h at 170 K and 4.45 e^2/h at 260 K. The emergence of a minimum value near 110 K followed by stabilisation toward an approximately consistent value above this temperature is inconsistent with continuous monotonic thermal decay. Panel B of Figure 2 presents σ_Q across the temperature range, illustrating the minimum near 110 K and the subsequent stabilisation of transport behaviour across device configurations of varying cleanliness.

Viscosity-to-entropy ratio behaviour: The viscosity-to-entropy ratio η/s decreases rapidly from approximately 14,559 at 100 K through 1,305 at 110 K and 501 at 115 K, approaching comparatively stable values near the holographic bound above approximately 120 K. The rapid decrease concentrated near 110 K is followed by stabilisation rather than continued smooth power-law decrease, as would be expected under conventional scattering-dominated transport behaviour. Panel C of Figure 2 presents η/s across the measured temperature range for the D1S5 ultraclean device, with the holographic bound value indicated [9].

Thermal smearing behaviour: The thermal smearing width n_0 normalised to temperature yields a ratio n_0/T of approximately $0.174 \times 10^{12} \text{ cm}^{-2} \text{ K}^{-1}$ at 19 K, decreasing to $0.127 \times 10^{12} \text{ cm}^{-2} \text{ K}^{-1}$ at 30 K and $0.100 \times 10^{12} \text{ cm}^{-2} \text{ K}^{-1}$ at 60 K, before increasing significantly to $0.200 \times 10^{12} \text{ cm}^{-2} \text{ K}^{-1}$ at 110 K and then decreasing again

to $0.147 \times 10^{12} \text{ cm}^{-2} \text{ K}^{-1}$ at 170 K and $0.123 \times 10^{12} \text{ cm}^{-2} \text{ K}^{-1}$ at 260 K. The factor of two increase in n_0/T between 60 K and 110 K, occurring within the same temperature window as the anomalies in the other three observables, is not consistent with the expectation of constant n_0/T under linear thermal smearing behaviour. Panel D of Figure 2 presents n_0/T across the temperature range, with the expected constant value indicated for reference.

5.4 Effective Kernel Time Scale Extracted from Minimum Conductivity

The extraction procedure for the dimensionless ratio τ_m/τ_p from minimum conductivity was derived in Section 4.2 and is applied here to the Majumdar dataset. The procedure assumes an exponential interaction kernel $K(\Delta\tau) = (1/\tau_m)\exp(-\Delta\tau/\tau_m)$, adopts G_{\min} as the observable proxy for kernel-weighted propagation efficiency at the charge neutrality point, and expresses the internal kernel memory scale τ_m as a dimensionless ratio relative to the external Planckian reference scale $\tau_p = \hbar/k_{\text{BT}}$ through:

$$\frac{\tau_m}{\tau_p} = G_{\min} \left(\frac{L}{W} \right) \frac{h}{4e^2}$$

where L/W is the inverse aspect ratio of the device channel and the factor of four reflects graphene's fourfold spin-valley degeneracy. This ratio is an observational correspondence connecting the framework's internal kernel memory scale to SI measurement, as established in Section 4.2, rather than an identification of the decay progression coordinate τ with clock time.

The ratio τ_m/τ_p extracted from G_{\min} across the experimental temperature range decreases monotonically from 0.901 at 90 K through 0.820 at 110 K to 0.440 at 249 K, as presented in Figure 3. The ratio remains below unity across the full measured temperature range, indicating that the effective kernel weighting scale is consistently shorter than the Planckian thermal reference across all measured conditions. The decrease is well described by a power-law dependence $\tau_m/\tau_p \propto T^{-0.72}$, consistent with the temperature scaling behaviour characteristic of quantum critical systems in which observable quantities follow power-law rather than linear temperature dependencies. The exponent -0.72 implies that kernel memory weakens more slowly than the Planckian bound itself, which scales as T^{-1} , indicating that a residual structural contribution to interaction memory persists to higher temperatures before being fully overcome by thermal fluctuations.

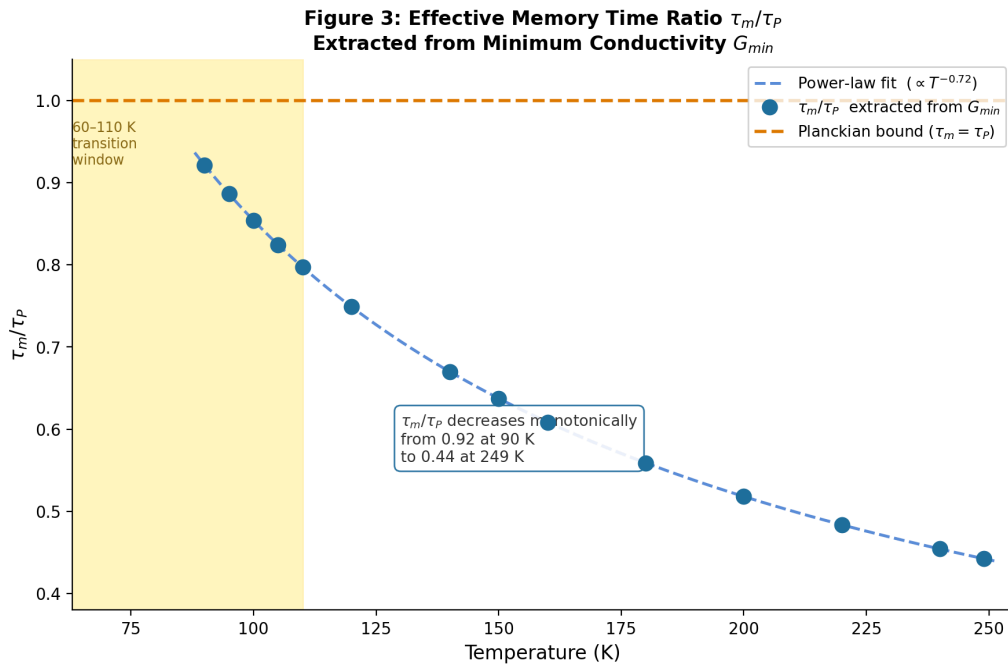


Figure 3. Effective memory time ratio τ_m/τ_p extracted from minimum conductivity.

The approach of the ratio toward unity as temperature decreases toward the lower limit of the measured range is consistent with the interpretation that effective kernel behaviour approaches the Planckian reference scale at low temperatures, though data below 90 K would be required to determine whether the ratio

saturates toward a stable low-temperature value or continues to approach unity. This represents the first experimental opportunity identified in Section 7.3.

The extracted τ_m values are presented as effective proxy parameters under the simplified exponential kernel assumption rather than as uniquely determined microscopic quantities. The sensitivity of this extraction to alternative kernel forms represents an open direction for future refinement, as noted in Section 7.

5.5 Interpretation Within the Non-Stationary Kernel Framework

The synchronized anomalous behaviour observed across four independent transport observables within the localized temperature window between 60 K and 110 K is interpreted within the present framework as a signature of non-stationary effective kernel evolution associated with a localized transition regime. Within the entropy-decay curvature framework, this corresponds to a transition from the stable-regime condition $dK_{\text{eff}}/d\tau \approx 0$ and $dK_{\text{eff}}/d\Psi \approx 0$ toward a regime in which both kernel variation indicators become non-negligible, shifting the balance between the $\alpha(K)$, $\beta(K)$, and $\gamma(K)$ propagation contributions and producing the synchronized observable deviations identified in Section 5.3. The simultaneous deviation of G_{min} scaling, Lorenz ratio rate behaviour, σ_Q minimum, η/s stabilisation, and n_0/T increase within a consistent temperature window provides convergent indirect evidence that the effective interaction weighting structure governing graphene transport undergoes localized evolution within this regime.

A contribution from resonant kernel coupling cannot be excluded on the basis of the present analysis. The comparatively sharp character of the σ_Q minimum near 110 K and the abrupt reversal in n_0/T behaviour at the same temperature are consistent with the possibility that the effective propagation rate associated with environmental background interaction approaches compatibility with the internal decay progression governing graphene subsystem response near this temperature, producing a localized enhancement of $dK_{\text{eff}}/d\Psi$. The distinction between threshold-induced and resonant kernel coupling mechanisms within the present dataset would require additional experimental investigation, as discussed in Section 6.

The observable transition from the low-temperature to the high-temperature transport regime does not require abrupt microscopic structural rearrangement or conventional thermodynamic phase separation in the present interpretation. Instead, the observable transport anomalies emerge through localized evolution of the effective interaction weighting structure governing entropy propagation, producing synchronized deviations across multiple transport observables within a finite temperature interval without requiring the formation of a new equilibrium phase in the conventional thermodynamic sense.

5.6 Consilience of Independent Approaches Toward a Unified Physical Picture

The transport behaviour of ultraclean graphene near the Dirac point, as reported by Majumdar and coworkers [3], presents a system in which conventional stationary scattering descriptions become insufficient and multiple independent observables deviate simultaneously within a localised temperature window. The entropy-decay curvature framework developed in the present work interprets this behaviour as a signature of evolving interaction-weighting structure, a non-stationary effective kernel whose memory scale, extracted from minimum conductivity as the dimensionless ratio τ_m/τ_p , decreases monotonically from 0.901 at 90 K to 0.440 at 249 K following a power-law $T^{-0.72}$, remaining sub-Planckian across the full measured range. Independently, and from an entirely different starting point, Patel, Lunts and Albergo [4] arrive at a compatible picture through numerically exact simulation of a microscopic spin-fermion model with spatially disordered interactions: their strange-metal phase produces a universal Planckian transport coefficient $\alpha_0 \approx 0.4$ that is independent of coupling strength, emerges from an extended gapless phase rather than a sharp critical point, and is carried by a fermion sector that remains clean and spatially extended despite strong disorder in the bosonic sector. These three approaches: experimental measurement, phenomenological entropy-decay framework, and microscopic numerical simulation, proceed from different foundations, speak different languages, and make different assumptions. Yet they converge on the same physical picture: that transport anomalies in strongly interacting low-dimensional systems reflect the evolution of interaction-weighting structures operating on sub-Planckian timescales [8] within extended transition-sensitive regimes, rather than the crossing of sharp phase boundaries or the onset of new microscopic order. That this convergence is reached independently, without any of the three approaches

being designed to agree with the others, is the strongest available evidence that the picture is capturing something real. The present analysis establishes that the synchronized transport anomalies observed in ultraclean graphene are consistent with this picture. It does not constitute proof. Establishing proof is the work of the experimental opportunities identified in Section 7.

6. Experimental Implications of Transition Mechanism Distinction

The two transition mechanisms introduced in Section 3.4 and interpreted within the graphene transport analysis of Section 5 carry distinct experimental implications that extend beyond the present dataset. Although both threshold-induced kernel evolution and resonant kernel coupling may produce externally similar transport anomalies, including suppressed conductivity, synchronized multi-observable deviation, and localized regime transitions, the underlying interaction-kernel dynamics governing each mechanism differ in ways that should produce distinguishable signatures under controlled experimental conditions. The present section develops these distinctions and identifies experimental approaches through which the two mechanisms may be separated.

6.1 Distinguishing Threshold-Induced from Resonant Kernel Evolution

Threshold-induced kernel evolution is driven primarily through accumulated subsystem interaction. Observable transition behaviour is therefore expected to exhibit strong dependence on interaction history, including environmental loading duration, thermal history, and the rate at which external drive is introduced into the subsystem. Because the effective interaction weighting structure evolves progressively as accumulated interaction destabilises the existing stationary regime, observable anomalies are expected to emerge gradually as the subsystem approaches the transition-sensitive interval. Recovery following the transition is similarly expected to be gradual, reflecting the time required for the subsystem interaction weighting structure to stabilise into a new approximately stationary regime.

Resonant kernel coupling, by contrast, is driven primarily through compatibility between incoming propagation structure and the internal decay progression governing subsystem response. Observable anomalies associated with resonant coupling are therefore expected to emerge more abruptly and within comparatively narrow sensitivity windows relative to threshold-dominated evolution. Comparatively modest changes in externally controlled propagation parameters, the frequency structure, drive coupling geometry, or propagation mode, may produce disproportionately strong transport responses once propagation compatibility approaches a localized coupling condition. Recovery behaviour following resonant coupling is similarly expected to be sharper than threshold-dominated recovery, reflecting changes in propagation compatibility rather than progressive environmental accumulation.

These distinctions suggest that the two mechanisms should respond differently to controlled experimental variation. Threshold-sensitive evolution is expected to depend strongly on environmental loading rate and accumulated drive history, while resonant coupling should depend primarily on the spectral and structural character of the incoming propagation relative to the internal subsystem progression. Varying external drive intensity, loading rate, subsystem geometry, and propagation frequency structure independently should therefore allow comparison between threshold-sensitive and resonance-sensitive transport responses under otherwise similar observable conditions.

Within the kernel variation framework established in Sections 3 and 4, these two situations correspond to distinct behaviours of the kernel evolution indicators. Threshold-induced evolution is characterised primarily by a non-negligible $dK_{\text{eff}}/d\tau$, the kernel weighting structure changes as accumulated decay progression destabilises the existing stationary regime, while the interaction structure configuration Ψ remains comparatively stable. Resonant kernel coupling, by contrast, is characterised primarily by a non-negligible $dK_{\text{eff}}/d\Psi$, the propagation structure becomes sensitive to configuration at the point of compatibility between incoming propagation and internal decay progression, even when accumulated interaction history remains limited. These distinct signatures in the kernel variation indicators suggest that the two mechanisms may in principle be separated not only through external drive variation as developed in Section 6.2, but through

systematic analysis of how transport anomalies evolve as a function of interaction history versus propagation structure configuration.

6.2 Application to the Graphene Transition Window and Open Experimental Directions

Within the graphene transport interpretation developed in Section 5, the localized anomalies observed between 60 K and 110 K may phenomenologically contain contributions from both mechanisms simultaneously. The gradual suppression of transport observables approaching the transition window from below is broadly consistent with progressive threshold-sensitive destabilisation of the low-temperature interaction weighting regime. The comparatively sharp resolution of the σ_Q minimum near 110 K and the abrupt reversal in n_0/T at the same temperature suggest that partial resonant kernel coupling may additionally contribute within the transition interval, producing the localized and synchronized character of the observed anomalies.

The present framework identifies three experimental directions through which the mechanism distinction may be further investigated.

First, transport measurements extending below 19 K would determine whether the power-law dependence $\tau_m/\tau_p \propto T^{-0.72}$ identified in Section 5.4 continues toward lower temperatures, saturates toward a stable low-temperature value, or steepens into a qualitatively different functional form, each possibility carrying distinct implications for the nature of kernel evolution as developed in Opportunity 1 of Section 7.3. Saturation toward a stable low-temperature value would be more consistent with threshold-dominated stabilisation into a fixed low-temperature interaction weighting regime, while continued or steepening power-law decrease would suggest that the low-temperature kernel regime has not yet been reached within the experimentally accessible range.

Second, systematic variation of external drive frequency and coupling geometry at fixed temperature near the transition window would test whether transport anomalies exhibit narrow propagation-sensitive windows consistent with resonant coupling or broad drive-independent behaviour consistent with threshold accumulation.

Third, comparison of the transition window temperature across ultraclean graphene devices of different geometry and environmental conditions would test whether the crossover is universal, consistent with an intrinsic subsystem interaction structure, or device-dependent, consistent with threshold-sensitive environmental accumulation.

These experimental directions are not proposed as definitive tests of the entropy-decay curvature framework as a whole. Rather, they represent targeted measurements capable of distinguishing between the two transition mechanisms proposed within the framework, providing a basis for refining the phenomenological interpretation of localized kernel evolution in graphene transport and potentially in other systems exhibiting similar synchronized multi-observable anomalies near localized transition regimes.

The universality of the Planckian transport coefficient across coupling strengths found by Patel, Lunts and Albergo [4] in their numerical modelling of two-dimensional metals with disordered interactions offers indirect evidence bearing on this mechanism distinction. Their result that the transport scattering rate at $\lambda = \lambda_s$ remains $\alpha_0 \approx 0.4 \cdot k_{BT}/\hbar$ independent of the strength of the disordered Yukawa coupling, is broadly consistent with a threshold-induced rather than resonant origin for the dominant transition mechanism in that system. A scattering rate that is independent of coupling strength suggests that the transition is governed by accumulated subsystem interaction history rather than by the precise compatibility between propagation structure and internal decay progression, which would be expected to vary with coupling strength. Whether the graphene transition window exhibits similar coupling-strength independence, testable through systematic variation of device geometry and environmental conditions as proposed in the third experimental direction above, would provide a direct comparison point between the two systems and further constrain the mechanism identification within the present framework.

7. Limitations, Open Correspondence, and Opportunities

The entropy-decay curvature framework developed in the present work extends the original Tsang equation formalism through memory-embedded subsystem interaction, effective kernel emergence, and non-stationary kernel promotion, arriving at a unified interpretive structure capable of describing localised transport-regime evolution within a single evolving-kernel formalism. Several important limitations define the current boundaries of this formalism and motivate the directions for future development identified in Section 7.3. These limitations are stated here not as apologies but as precise demarcations of what the present work establishes and what remains open, a distinction that is itself part of the framework's intellectual commitment to honest phenomenological development.

7.1 Limitations

Phenomenological rather than first-principles foundation: The effective interaction kernel K_{eff} is introduced through subsystem decomposition under experimentally constrained conditions rather than derived from a microscopic or first-principles treatment of material structure. The functional forms of the individual subsystem coupling kernels K_{GE} and K_{GD} are not derived within the present framework, and the kernel evolution function governing non-stationary behaviour remains unspecified beyond qualitative characterisation through $dK/d\tau$ and $dK/d\Psi$. The framework therefore provides a structural description of how kernel evolution produces observable transport anomalies without yet providing a quantitative predictive model of the kernel evolution itself.

Absence of unit definition for the effective kernel: The effective interaction kernel K_{eff} is treated throughout the present work as a dimensionless interaction weighting structure characterising relative subsystem coupling history. No absolute unit system has been established within the framework connecting K_{eff} to conventional physical quantities such as conductivity, scattering rate, or thermodynamic state variables in a dimensionally closed manner. The extracted proxy measures of effective kernel behaviour presented in Section 5 therefore represent relative indicators of interaction weighting evolution rather than absolute determinations of a fully defined physical quantity.

Indirect observability through transport proxies: The effective interaction kernel is not directly observable as an isolated quantity within the present experimental configuration. Its behaviour must be inferred indirectly through transport observables such as minimum conductivity, Lorenz ratio, viscosity-to-entropy ratio, and thermal smearing, each of which reflects a different projection of the underlying interaction weighting structure. The convergence of anomalous behaviour across four independent proxy observables within a consistent temperature window provides convergent indirect evidence of kernel evolution, but does not uniquely determine the kernel evolution function or exclude alternative transport interpretations.

Single dataset and limited temperature range: The empirical application developed in Section 5 is restricted to the Majumdar dataset spanning temperatures from 19 K to 260 K in ultraclean hBN-encapsulated graphene. The behaviour of transport observables below 19 K, which would be required to determine whether the effective kernel time scale saturates toward a stable low-temperature value or continues evolving, remains unexamined within the present work. The universality of the localized transition window across different material systems, device geometries, and environmental conditions has not been established.

Mechanism distinction remains qualitative: The two transition mechanisms proposed in Section 6, the threshold-induced kernel evolution and the resonant kernel coupling, are distinguished within the present framework on phenomenological grounds. The present dataset does not permit unambiguous separation of the two contributions, and the relative magnitude of each mechanism within the observed graphene transition window remains unquantified. The framework does not yet provide a quantitative criterion for determining which mechanism dominates under specific experimental conditions.

7.2 Open Correspondence

Between entropy-decay coordinates and conventional observables: The open correspondence problem between entropy-decay framework coordinates and conventional SI measurement units was partially and deliberately engaged in Section 4.2 through the extraction of the dimensionless ratio τ_m/τ_p from minimum conductivity. That extraction represents the first concrete instance within the present work of the broader correspondence challenge described here: the decay progression coordinate τ was connected to measurable quantities: minimum conductance, device geometry, and the quantum of conductance, through a limited and explicitly stated observational correspondence rather than through a foundational identification of framework coordinates with conventional spacetime units. The factor \hbar introduced in Section 4.2 served as a dimensional bridge rather than a claim that τ is clock time. The Planckian timescale τ_p was introduced as an external measuring rod rather than a framework concept. This approach, making observational correspondences explicit, local, and limited, is the methodological stance the framework adopts toward the broader problem described below, and Section 4.2 demonstrates that meaningful quantitative contact with experimental data is achievable within that stance even before a formally closed dimensional correspondence has been established.

Within the present framework, the decay progression coordinate τ and the interaction structure coordinate Ψ are not introduced as direct replacements for conventional SI quantities such as temporal duration or spatial displacement. Rather, they represent internal descriptors of entropy-decay evolution and subsystem interaction structure whose observable correspondences with conventional measurable quantities including temperature, carrier density, transport time scales, and propagation length scales, are treated phenomenologically within the present work rather than assumed axiomatically.

The framework does not presently establish a closed dimensional correspondence between entropy-decay coordinates and conventional spacetime unit systems. This should not be interpreted solely as mathematical incompleteness. Rather, it reflects the underlying assumption of the entropy-decay curvature framework that conventional spacetime decomposition may itself emerge from more fundamental entropy-decay relations rather than acting as the primary ontological structure governing physical description. Establishing a consistent and formally closed observational correspondence between entropy-decay framework coordinates and conventional measurable quantities therefore remains an open problem for future development, and one whose resolution may require extension of the framework toward the foundational level at which conventional coordinate systems themselves are treated as emergent rather than assumed.

7.3 Opportunities

Each limitation identified above defines a concrete direction through which the present framework may be extended, tested, and refined. Three primary opportunities are identified corresponding to the most experimentally accessible and theoretically significant open problems within the current formalism.

Opportunity 1 – Determining the functional form of kernel evolution through low-temperature transport measurements

The effective kernel memory scale ratio τ_m/τ_p follows a power-law dependence $\tau_m/\tau_p \propto T^{-0.72}$ across the measured temperature range from 90 K to 249 K, decreasing monotonically from 0.901 to 0.440. Whether this power-law behaviour continues below 90 K, saturates toward a stable low-temperature value, or steepens into a different functional form remains undetermined within the present dataset. Each possibility carries distinct theoretical implications. Continued power-law decrease would suggest that the kernel memory scale tracks a temperature-dependent structural contribution that persists without saturation toward lower temperatures, implying no stable low-temperature kernel regime within the experimentally accessible range. Saturation toward a stable low-temperature value, producing a sigmoid functional form for kernel evolution, would be consistent with threshold-dominated stabilisation into a fixed low-temperature interaction weighting regime, and would provide a direct constraint on the threshold energy scale governing kernel evolution. A steepening of the decrease, departing from the power-law form, would suggest the onset of a qualitatively different kernel evolution regime at low temperatures, potentially associated with a crossover in the dominant propagation channel from $\beta(K)$ -mediated scattering behaviour toward a different

propagation structure. Transport measurements in ultraclean graphene extending below 19 K, ideally to below 10 K, in the same experimental geometry as the Majumdar dataset would provide a direct discriminator between these three possibilities without requiring any new theoretical development beyond what has already been established in the preceding sections. This single measurement represents the highest-priority experimental opportunity identified by the present framework.

Opportunity 2 – Testing universality of the transition window across graphene devices and material systems

Within the present framework, the effective interaction kernel K_{eff} represents the consolidated interaction weighting structure of the graphene subsystem under specific environmental and drive conditions. If the transition window between 60 K and 110 K reflects an intrinsic property of the graphene interaction weighting structure rather than device-specific environmental accumulation, its location should remain consistent across ultraclean graphene devices of different geometry, substrate conditions, and environmental configurations when measured under equivalent drive conditions. Systematic comparison of the transition window temperature across existing ultraclean graphene datasets from independent experimental groups would therefore provide a direct test of whether the observed anomalies reflect a universal property of the graphene interaction weighting structure or a threshold-sensitive response to device-specific environmental conditions. A consistent transition temperature across devices of varying cleanliness and geometry would strongly support the interpretation that kernel evolution near 110 K reflects an intrinsic subsystem interaction property rather than accumulated environmental sensitivity. Extension of this comparison to other two-dimensional material systems exhibiting quantum critical transport behaviour would further test whether the non-stationary kernel framework captures a general feature of interaction-dominated transport beyond the specific case of graphene.

Opportunity 3 – Separating threshold-induced and resonant kernel coupling through controlled drive variation

As established in Section 6, threshold-induced kernel evolution and resonant kernel coupling are expected to produce distinguishable experimental signatures under controlled conditions. Threshold-dominated evolution should depend strongly on accumulated environmental interaction history and exhibit gradual onset behaviour sensitive to loading rate and thermal history. Resonant kernel coupling should instead depend primarily on the spectral and structural character of the incoming propagation relative to the internal subsystem decay progression, exhibiting comparatively abrupt onset within narrow propagation-sensitive windows and responding disproportionately to modest changes in drive frequency or coupling geometry. Systematic variation of external drive frequency, coupling geometry, and environmental loading rate at fixed temperature near the transition window, while monitoring the four transport observables identified in Section 5, would allow direct comparison between these expected signatures. A narrow frequency window within which transport anomalies are significantly enhanced relative to broad-spectrum drive conditions would support resonant kernel coupling as a contributing mechanism. Broad drive-independent onset behaviour would instead support threshold accumulation as the dominant mechanism. This experimental direction requires no new sample fabrication beyond what has already been demonstrated in the Majumdar configuration [3] and could in principle be implemented within existing ultraclean graphene measurement platforms.

8. Conclusion

The present work has developed an extension of the entropy-decay curvature framework through the introduction of dynamically evolving non-stationary interaction kernels emerging from explicit subsystem interaction decomposition. Beginning from the foundational entropy-decay curvature relation expressed through the Tsang equation, the framework has been extended progressively through stationary memory-embedded formalism, subsystem interaction decomposition, and non-stationary kernel promotion, arriving at a unified formalism capable of representing localised transport-regime evolution within a single evolving-kernel structure. Throughout this development, two methodological commitments have been

maintained. The first is that observable transport quantities are treated as emergent consequences of stabilised kernel regimes rather than as independently fundamental inputs to the framework. The second is that quantitative contact with experimental data is made through explicit and limited observational correspondences concretely, through the dimensionless ratio τ_m/τ_p extracted from minimum conductivity in Section 4.2, rather than through foundational identifications of framework coordinates with conventional SI units. These commitments distinguish the present framework from both purely descriptive phenomenology and from microscopically derived transport theories, positioning it as a structural interpretive framework whose boundaries are clearly stated and whose directions for extension are explicitly identified.

The central mathematical advancement of the present work is the promotion of the stationary interaction kernel $K(\tau-\tau')$ into a non-stationary effective kernel $K_{\text{eff}}(\tau-\tau', \tau)$ emerging naturally from subsystem decomposition under experimentally constrained conditions. This promotion is not introduced as an arbitrary extension of the existing formalism. Rather, it emerges directly from the recognition that the graphene subsystem evolves under simultaneous coupling to an approximately stationary environmental background and an externally controlled drive subsystem, and that the effective interaction weighting governing observable transport behaviour consolidates both coupling contributions through $K_{\text{eff}} = K_{\text{GE}} + K_{\text{GD}}$. Within stable transport regimes, this effective kernel evolves negligibly and the earlier stationary memory-embedded formalism is recovered naturally as a limiting case. Near localized transition conditions, the effective kernel evolves non-negligibly and observable transport anomalies emerge as consequences of interaction weighting reorganisation rather than as independent dissipative corrections external to the entropy-decay curvature dynamics.

That this interpretation is reached independently from, and found to be broadly consistent with, the results of numerically exact microscopic simulation of disordered quantum critical metals [4], a body of work proceeding from entirely different foundations and making no use of entropy-decay curvature dynamics, strengthens the case that the physical picture described here captures a genuine feature of strongly interacting transport systems rather than an artefact of any particular theoretical construction.

The entropy-decay curvature framework does not claim to replace or invalidate existing transport descriptions developed within condensed matter physics. Rather, it proposes that certain localized transport anomalies may be coherently interpreted through evolving subsystem interaction weighting structures operating within a broader entropy-decay formalism, and that this interpretation opens experimentally accessible directions for investigating the boundary between stable and transition-sensitive transport regimes. The present work establishes that the synchronized transport anomalies observed in ultraclean graphene near the Dirac point are consistent with this interpretation, and that the non-stationary kernel formalism provides a phenomenologically coherent framework for connecting entropy-decay curvature dynamics, subsystem interaction, memory effects, and localized regime transition within a unified evolving-kernel structure.

The present work represents one step in that extension. Its boundaries are clearly stated, its directions for further development are explicitly identified, and its central finding that the synchronized transport anomalies observed in ultraclean graphene near the Dirac point are consistent with localised non-stationary kernel evolution operating within the entropy-decay curvature formalism, is supported not only by the convergence of four independent transport observables within a single transition window, but by its independent alignment with the broader picture of Planckian transport emerging from extended interaction-sensitive phases that is taking shape across experimental, phenomenological, and numerical approaches to strongly interacting transport systems. The Tsang equation [1,2] remains the foundational dynamical principle throughout. What the present work adds is one more line of evidence that this principle, and the evolving-kernel formalism built from it, are oriented in the right direction.

Data Availability Statement

No new data were created or analyzed in this study. Data sharing is not applicable to this article.

Acknowledgments

The author thanks the reviewers and peers for constructive discussions that improved the clarity of the manuscript. Large language models (ChatGPT, Claude) were used for language refinement and formatting only; all scientific concepts and equations were developed independently by the author.

Author Contributions: CRediT

Conceptualization, L.H.L. Tsang; Methodology, L.H.L. Tsang; Formal analysis, L.H.L. Tsang; Investigation, L.H.L. Tsang; Writing—original draft, L.H.L. Tsang; Writing—review & editing, L.H.L. Tsang; Visualization, L.H.L. Tsang.

Funding sources

This research did not receive any specific grant from funding agencies in the public, commercial, or not-for-profit sectors.

Declaration of generative AI and AI-assisted technologies in the manuscript preparation process

During the preparation of this work the author(s) used ChatGPT, and Claude to refine and format language. After using this tool/service, the author(s) reviewed and edited the content as needed and take(s) full responsibility for the content of the published article.

References

- [1] Tsang, L. H. L. *The Entropy-Decay Universe: Redefining Time, Force, and Structure in Modern Physics* (2025). ISBN-13: 979-8281924375
- [2] Tsang, L. H. L. *Beyond the Standard Model: An Advanced Study of the Bottlenecks in Modern Science through Higher-Level Entropy-Decay Theory and Equations*, Version 2.0 (2025). ISBN-13: 979-8283077819
- [3] Majumdar, A., Chadha, N., Pal, P., Gugnani, A., Ghawri, B., Watanabe, K., Taniguchi, T., Mukerjee, S. & Ghosh, A. Universality in quantum critical flow of charge and heat in ultraclean graphene. *Nat. Phys.* 21, 1374–1379 (2025). <https://doi.org/10.1038/s41567-025-02972-z>
- [4] Patel, A. A., Lunts, P., & Albergio, M. S. Strange metals and Planckian transport in a gapless phase from spatially random interactions. *Phys. Rev. X* 15, 031064 (2025). <https://doi.org/10.1103/611k-yxb9>
- [5] Crossno, J. *et al.* Observation of the Dirac fluid and the breakdown of the Wiedemann–Franz law in graphene. *Science* 351, 1058–1061 (2016). <https://doi.org/10.1126/science.aad0343>
- [6] Lucas, A. & Surówka, P. Hydrodynamics of electrons in graphene. *Phys. Rev. B* 97, 245128 (2018). <https://doi.org/10.1103/PhysRevB.97.245128>
- [7] Principi, A. & Vignale, G. Violation of the Wiedemann–Franz law in hydrodynamic electron liquids. *Phys. Rev. Lett.* 115, 056603 (2015). <https://doi.org/10.1103/PhysRevLett.115.056603>
- [8] Cao, Y. *et al.* Strange metal in magic-angle graphene with near Planckian dissipation. *Phys. Rev. Lett.* 124, 076801 (2020). <https://doi.org/10.1103/PhysRevLett.124.076801>
- [9] Kovtun, P. K., Son, D. T. & Starinets, A. O. Viscosity in strongly interacting quantum field theories from black hole physics. *Phys. Rev. Lett.* 94, 111601 (2005). <https://doi.org/10.1103/PhysRevLett.94.111601>
- [10] Zwanzig, R. Memory effects in irreversible thermodynamics. *Phys. Rev.* 124, 983–992 (1961). <https://doi.org/10.1103/PhysRev.124.983>
- [11] Mori, H. Transport, collective motion, and Brownian motion. *Prog. Theor. Phys.* 33, 423–455 (1965). <https://doi.org/10.1143/PTP.33.423>
- [12] Kupčić, I. Memory-function approach to the theory of the optical conductivity of interacting electrons. *Phys. Rev. B* 95, 205101 (2017). <https://doi.org/10.1103/PhysRevB.95.035403>
- [13] Lucas, A., Crossno, J., Fong, K. C., Kim, P. & Sachdev, S. Transport in inhomogeneous quantum critical fluids and in the Dirac fluid in graphene. *Phys. Rev. B* 93, 075426 (2016). <https://doi.org/10.1103/PhysRevB.93.075426>
- [14] Bandurin, D. A. *et al.* Negative local resistance caused by viscous electron backflow in graphene. *Science* 351, 1055–1058 (2016). <https://doi.org/10.1126/science.aad0201>
- [15] Torre, I., Tomadin, A., Geim, A.K. & Polini, M. Nonlocal transport and the hydrodynamic shear viscosity in graphene. *Phys. Rev. B* 92, 165428 (2015). <https://doi.org/10.1103/PhysRevB.92.165433>
- [16] Alberte, L., Baggioli, M., Pujolàs, O. & Salmi, P. Viscosity bound violation in holographic solids and the viscoelastic response. *J. High Energ. Phys.* 2016, 74 (2016). [https://doi.org/10.1007/JHEP07\(2016\)074](https://doi.org/10.1007/JHEP07(2016)074)